Nuclear Engineering and Technology 53 (2021) 603–610

Contents lists available at ScienceDirect

Nuclear Engineering and Technology

journal homepage: www.elsevier.com/locate/net

Original Article

Characterization and thermophysical properties of $Zr_{0.8}Nd_{0.2}O_{1.9}$–MgO composite

Chiranjit Nandi [a, *], Santu Kaity [a, c], Dheeraj Jain [b, c], V. Grover [b, c], Amrit Prakash [a, c], P.G. Behere [a]

[a] Radiometallurgy Division, Bhabha Atomic Research Centre, Mumbai, 400 085, India
[b] Chemistry Division, Bhabha Atomic Research Centre, Mumbai, 400 085, India
[c] Homi Bhabha National Institute, Mumbai, 400 094, India

ARTICLE INFO

Article history:
Received 3 January 2020
Received in revised form
6 July 2020
Accepted 15 July 2020
Available online 29 July 2020

Keywords:
$Zr_{0.8}Nd_{0.2}O_{1.9}$–MgO composites
XRD
Thermal expansion
Specific heat
Thermal conductivity

ABSTRACT

The major drawback of zirconia-based materials, in view of their applications as targets for minor actinide transmutation, is their poor thermal conductivity. The addition of MgO, which has high thermal conductivity, to zirconia-based materials is expected to improve their thermal conductivity. On these grounds, the present study aims at phase characterization and thermophysical property evaluation of neodymium-substituted zirconia ($Zr_{0.8}Nd_{0.2}O_{1.9}$; using Nd_2O_3 as a surrogate for Am_2O_3) and its composites with MgO. The composite was prepared by a solid-state reaction of $Zr_{0.8}Nd_{0.2}O_{1.9}$ (synthesized by gel combustion) and commercial MgO powders at 1773 K. Phase characterization was carried out by X-ray diffraction and the microstructural investigation was performed using a scanning electron microscope equipped with energy dispersive spectroscopy. The linear thermal expansion coefficient of $Zr_{0.8}Nd_{0.2}O_{1.9}$ increases upon composite formation with MgO, which is attributed to a higher thermal expansivity of MgO. Similarly, specific heat also increases with the addition of MgO to $Zr_{0.8}Nd_{0.2}O_{1.9}$. Thermal conductivity was calculated from measured thermal diffusivity, temperature-dependent density and specific heat values. Thermal conductivity of $Zr_{0.8}Nd_{0.2}O_{1.9}$–MgO (50 wt%) composite is more than that of typical UO_2 fuel, supporting the potential of $Zr_{0.8}Nd_{0.2}O_{1.9}$–MgO composites as target materials for minor actinides transmutation.

1. Introduction

Incineration of long-lived minor actinides (MAs) in nuclear reactors and accelerator-driven sub-critical systems (ADSS) has been considered as a promising option to reduce the radio-toxicity of nuclear waste significantly [1,2]. In this direction, a uranium-free inert matrix fuel (IMF) concept has been envisaged to burn minor actinides [3–6]. Several materials, which include oxides, carbides, nitrides, alloys and even composites, have been proposed and investigated as IMF [4]. CeO_2, MgO, $MgAl_2O_4$, YSZ and ZrO_2 have been considered as potential candidates for oxide-based inert matrix materials [4,7]. Among these oxides, zirconia-based materials have been found to be the most promising inert matrix candidate owing to their superior properties such as chemical and radiation stability, low neutron capture cross-section, good compatibility with reactor components etc. [8].

Considering the potential of ZrO_2 as a matrix component and Nd_2O_3 as a non-radioactive surrogate for minor actinides (namely, Am_2O_3 and Cm_2O_3), phase relations and thermophysical properties in ZrO_2–Nd_2O_3 binary system have been thoroughly investigated [9]. The reason for choosing Nd_2O_3 as a surrogate of Am_2O_3 and Cm_2O_3 has been discussed in detail elsewhere [9,10]. The phase relation studies indicated structural feasibility for loading a significant amount of trivalent minor actinides (20–50 mol.%) in ZrO_2 while maintaining a single-phase cubic structure. It must be mentioned that 20 mol.% Nd^{3+} substituted ZrO_2 ($Zr_{0.8}Nd_{0.2}O_{1.9}$) forms cubic fluorite-type (F-type) phase while 50 mol.% Nd^{3+} substituted ZrO_2 ($Nd_2Zr_2O_7$) exhibits pyrochlore-type structure. Though the pyrochlore-type phase contains much higher concentration of MAs as compared to the F-type phase, it exhibited poorer radiation stability as compared to the F-type phase [11–13]. The investigations on thermophysical properties clearly showed poor thermal conductivity (~1.6 $Wm^{-1}K^{-1}$) of $Zr_{0.8}Nd_{0.2}O_{1.9}$ sample over

* Corresponding author.
E-mail address: cnandi@barc.gov.in (C. Nandi).

https://doi.org/10.1016/j.net.2020.07.022

a wide temperature range (RT–1473 K) as compared to widely used typical oxide-based nuclear fuel such as UO_2 [9]. There are other reports in the literature as well, which also show lower thermal conductivity of Nd^{3+} substituted ZrO_2 ceramics such as $Zr_{0.7}Nd_{0.3}O_{1.85}$ [14,15] and $Nd_2Zr_2O_7$ [15,16]. Based on very close thermal conductivity of 1.5–2.0 $Wm^{-1}K^{-1}$ for all neodymium zirconates (20–50 mol.% Nd^{3+}-substituted ZrO_2) and better radiation response exhibited by F-type $Zr_{0.8}Nd_{0.2}O_{1.9}$ phase, $Zr_{0.8}Nd_{0.2}O_{1.9}$ was chosen to mimic the MAs bearing zirconia host phase in the present study.

The poor thermal conductivity is a major shortcoming of zirconia-based materials for their applications as inert matrix fuel. The use of these ceramics in reactors is expected to result in higher centreline temperature, large temperature gradients, thermal stresses, high fission gas release, low linear heat rating etc., which would adversely affect the in-pile performance of fuel matrix [6]. It is, therefore, very essential to improve the thermal conductivity of ZrO_2-based ceramics for their application as IMF. One possible strategy to improve thermal conductivity is an optimum addition of a secondary phase with higher thermal conductivity. Magnesium oxide (MgO) has been proposed as one such material to improve heat transport from oxide ceramic fuels because of its higher thermal conductivity as compared to UO_2 fuel [17]. Apart from high thermal conductivity, other favorable characteristics such as low neutron absorption cross-section, chemical stability, high melting point and high radiation stability of MgO justify its use in inert matrix fuels [18,19]. Although MgO is not compatible with hot water [20], which limits its use in light water reactors (LWRs), it has excellent compatibility with liquid metals, which are candidate coolant materials for fast reactors and ADSS [21]. Composites of MgO with ZrO_2 have also been investigated to achieve high thermal conductivity and better hot-water corrosion resistance for their use in LWRs [17]. Similarly, MgO–$Nd_2Zr_2O_7$ dual-phase inert matrix fuel has been reported to exhibit reasonable thermal conductivity of the composite matrix exploiting the high thermal conductivity of MgO [22]. Irradiation studies on MgO in MATINA and EFTTRA-T3 experiments have also indicated its satisfactory performance [23,24]. In a recent communication [11], we also reported that formation of a ceramic-ceramic composite of Nd-stabilised zirconia ($Zr_{0.8}Nd_{0.2}O_{1.9}$) with MgO enhances the radiation tolerance of $Zr_{0.8}Nd_{0.2}O_{1.9}$ phase against 120 MeV gold (Au) ion irradiation. It was also shown that the MgO phase shows better radiation tolerance out of the two phases in such composite. All these physicochemical properties of MgO are extremely relevant for its use in nuclear reactors.

The thermophysical properties of $Zr_{0.8}Nd_{0.2}O_{1.9}$–MgO composites have not been investigated to the best of our knowledge. Investigation of these properties, namely the bulk thermal expansion, specific heat capacity and thermal conductivity, on $Zr_{0.8}Nd_{0.2}O_{1.9}$ and its composite with MgO is the aim of the present study. It may be noted that $Zr_{0.8}Nd_{0.2}O_{1.9}$–MgO composite is a kind of dispersion fuel wherein the fuel fraction must be limited to 50 vol% [25]. Indeed, $MgAl_2O_4$–36 vol% UO_2 composite was chosen for irradiation in the SILOE reactor [26], while MgO–40 wt% UO_2, $MgAl_2O_4$–40 wt% UO_2 and Al_2O_3–40 wt% UO_2 composite has been irradiated under MATINA irradiations program [27]. On the same lines, an intermediate composition $Zr_{0.8}Nd_{0.2}O_{1.9}$–MgO (50 wt% or 36 vol% $Zr_{0.8}Nd_{0.2}O_{1.9}$) was chosen for the present study. The thermophysical properties of MgO, the other end member, have also been evaluated and reported for comparison with existing literature data.

2. Experimental

$ZrO(NO_3)_2.xH_2O$ (Loba Chemie, purity 99.5%), Nd_2O_3 (Indian Rare Earths Ltd., purity 99%), and MgO (Sigma-Aldrich, purity 99%) were used as starting materials. Hexahydrate stoichiometry of zirconyl nitrate (x = 6) was determined by thermo-gravimetric analysis. Gel combustion synthesis was employed to synthesize the nominal composition $Zr_{0.8}Nd_{0.2}O_{1.9}$. Nd_2O_3 and $ZrO(NO_3)_2\cdot 6H_2O$ were taken as the reactants and glycine was chosen as the fuel and the synthesis was carried out following the method reported elsewhere [9]. The fluffy powder produced by this route was calcined at 1073 K to remove residual carbonaceous impurities. Calcined $Zr_{0.8}Nd_{0.2}O_{1.9}$ and as-received MgO were employed to prepare $Zr_{0.8}Nd_{0.2}O_{1.9}$–MgO composite by conventional solid-state route, wherein these powders were mixed by pestle in an agate mortar in alcohol medium for 1 h. All powders were compacted in the form of pellets and sintered at 1773 K for 24 h in a static air atmosphere. The heating, as well as the cooling rates, were maintained at 5 K/min. Physical defects like cracks or end cap were not observed in the sintered pellets.

Phase analysis of sintered samples was carried out on a powder X-ray diffractometer using Cu K_α ($\lambda_{K\alpha1}$ = 1.5406 Å and $\lambda_{K\alpha2}$ = 1.5444 Å) radiation over two theta range from 10° to 80°. XRD patterns were analyzed by Rietveld and Le Bail refinement methods using the Fullprof program [28]. Microstructural analysis of sintered pellets was carried out using a scanning electron microscope (SEM) operated at 20 kV potential. The sample surface was coated with a thin layer of gold before recording the SEM images to avoid charging interference during the measurement. Images were recorded in both secondary electron (SE) (Everhart-Thornley detector) and backscattered electron (BSE) mode (solid-state backscattered electron detector). Energy dispersive spectroscopy (EDS, 80 mm^2, silicon drift detector) was used for elemental analysis of these pellets.

Bulk thermal expansion of sintered samples was measured in a high-temperature vertical dilatometer over the temperature range from RT to 1573 K using 10 K/min heating rate under flowing argon atmosphere (20 ml/min). Dilation was monitored by the movement of push-rod attached to an LVDT transducer. Specific heat of sintered samples was measured using a differential scanning calorimeter (DSC) under the flow of high purity argon (50 ml/min) over the temperature range from 300 K to 1073 K at 10 K/min heating rate. Thermal diffusivity of sintered samples was measured in a laser flash apparatus, under dynamic vacuum ($P < 1 \times 10^{-5}$ Torr) over the temperature range from RT to 1273 K at an interval of 100 K. Further details on specific heat and thermal diffusivity measurements are provided in our recent publications [9,14].

3. Results and discussion

3.1. Structural characterization

3.1.1. X-ray diffraction studies

Powder XRD patterns of $Zr_{0.8}Nd_{0.2}O_{1.9}$, MgO and their composite (50 wt%), after high-temperature sintering, are shown in Fig. 1. The nominal composition $Zr_{0.8}Nd_{0.2}O_{1.9}$ was found to exhibit fluorite-type (F-type) cubic phase (Space group: Fm-3m) while MgO showed NaCl-type (rock salt) crystal structure (Space group: Fm-3m). $Zr_{0.8}Nd_{0.2}O_{1.9}$–MgO composite was found to form a biphasic system consisting of NaCl-type MgO and F-type $Zr_{0.8}Nd_{0.2}O_{1.9}$ phase. Diffraction peaks corresponding to the $Zr_{0.8}Nd_{0.2}O_{1.9}$ phase shifted towards higher angles in the composite sample as compared to single-phase $Zr_{0.8}Nd_{0.2}O_{1.9}$ (shown in Fig. 1). This indicated a contraction of $Zr_{0.8}Nd_{0.2}O_{1.9}$ lattice, plausibly due to partial incorporation of aliovalent Mg^{2+} ions and the concomitant creation of oxygen ion vacancies in the lattice. From the reported ionic radii of constituent cations namely, Mg^{2+} (0.89 Å), Zr^{4+} (0.84 Å) and Nd^{3+} (1.109 Å) in eight-fold coordination [29], the average cationic radius in $Zr_{0.8}Nd_{0.2}O_{1.9}$ lattice is estimated to be

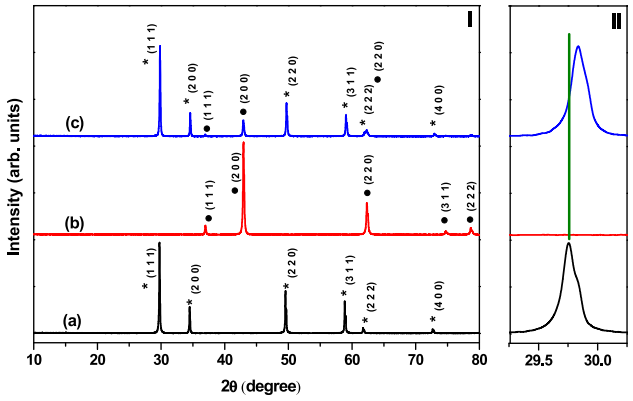

Fig. 1. (I) Room temperature XRD patterns of (a) $Zr_{0.8}Nd_{0.2}O_{1.9}$, (b) MgO and (c) $Zr_{0.8}Nd_{0.2}O_{1.9}$–MgO composite samples; (II) enlarged view of (111) peak of $Zr_{0.8}Nd_{0.2}O_{1.9}$ phase.

0.89 Å; similar to that of Mg^{2+}. Therefore, incorporation of Mg^{2+} in $Zr_{0.8}Nd_{0.2}O_{1.9}$ lattice is not expected to change the lattice parameter based on the sizes of host and guest cations. However, the introduction of associated oxygen ion vacancies (arising from charge balance requirement) would lead to lattice shrinkage. Details of the phases identified in different compositions and their lattice parameters, as determined by the refinement of powder diffraction patterns, are provided in Table 1. Lattice shrinkage of the $Zr_{0.8}Nd_{0.2}O_{1.9}$ phase in $Zr_{0.8}Nd_{0.2}O_{1.9}$–MgO composite sample, as compared to pure $Zr_{0.8}Nd_{0.2}O_{1.9}$ is also evident from lattice parameter values (Table 1). On the other hand, the lattice parameter of the MgO phase in $Zr_{0.8}Nd_{0.2}O_{1.9}$–MgO composite (4.2116 Å) is almost the same as that of pure MgO (4.2111 Å) sintered under identical conditions. This suggests that the MgO phase in the composite is present as almost pure MgO, and Zr^{4+} or Nd^{3+} incorporation in MgO lattice is not observed. Noguchi et al. [30], in their investigation on the MgO-rich region of the MgO–ZrO_2 system, also observed a constant lattice parameter (~4.211 Å) for MgO phase and attributed it to non-incorporation of ZrO_2 in MgO phase. Our present results are, therefore, in line with reported ones and indicate that MgO is present as a pure phase in the composite.

The phase fraction of $Zr_{0.8}Nd_{0.2}O_{1.9}$ as well as MgO in $Zr_{0.8}Nd_{0.2}O_{1.9}$–MgO (50 wt%) composite sample was determined by Rietveld refinement of powder XRD data using Fullprof-2011 program [28]. It may be noted that the XRD pattern indicated marginal solubility of Mg^{2+} in the F-type $Zr_{0.8}Nd_{0.2}O_{1.9}$ phase. The true composition of this F-type phase was estimated to be $Zr_{0.75}Nd_{0.19}Mg_{0.06}O_{1.845}$ according to EDS analysis (discussed later in the manuscript). Refinement was carried out using an appropriate structural model consisting of F-type $Zr_{0.75}Nd_{0.19}Mg_{0.06}O_{1.845}$ phase and NaCl-type MgO phase and an approximate scale parameter for these phases. Background fitting was carried out using a sixth-order polynomial function. Peak profile was modelled with the Pseudo-Voigt profile function. As-measured diffraction pattern, refined diffraction pattern and the difference plot between measured and refined patterns are shown in Fig. 2. Refinement parameters, namely R_p (8.44%), R_{wp} (12.7%) and goodness of fit (χ^2: 1.54), indicate that reasonably good fit has been achieved. Refinement results also indicated the presence of 51 ± 1 wt % $Zr_{0.75}Nd_{0.19}Mg_{0.06}O_{1.845}$ phase and 49 ± 1 wt% MgO, which is in excellent agreement with expected phase composition for $Zr_{0.8}Nd_{0.2}O_{1.9}$–MgO (50 wt%) composite.

Table 1
Different phases present in the samples and their lattice parameters.

Composition	Phases	Lattice parameter (Å)
$Zr_{0.8}Nd_{0.2}O_{1.9}$	Fluorite	5.2005 (2)
MgO	Rock salt	4.2111 (1)
$Zr_{0.8}Nd_{0.2}O_{1.9}$–MgO (50 wt%)	Fluorite ($Zr_{0.8}Nd_{0.2}O_{1.9}$)	5.1828 (2)
	Rock salt (MgO)	4.2116 (3)

3.1.2. Electron microscopy studies

The representative secondary electron micrographs of sintered $Zr_{0.8}Nd_{0.2}O_{1.9}$, MgO and $Zr_{0.8}Nd_{0.2}O_{1.9}$–MgO composite samples are shown in Fig. 3(a)-(c). All the sintered samples display a considerable fraction of open pores (the dark regions in the microstructure), which are distributed throughout the samples indicating that they are not highly dense. The BSE images indicate a single-phase microstructure for $Zr_{0.8}Nd_{0.2}O_{1.9}$ and MgO (Fig. 3(a) and (b)) and a two-phase microstructure for both $Zr_{0.8}Nd_{0.2}O_{1.9}$–MgO composite ((Fig. 3(c)) as expected. The light grey phase in Fig. 3(c) represents the MgO phase, while the bright phase corresponds to the $Zr_{0.8}Nd_{0.2}O_{1.9}$ phase. The BSE image also clearly indicates that the $Zr_{0.8}Nd_{0.2}O_{1.9}$ phase is homogeneously distributed in the MgO matrix or vice versa.

Average compositions in these samples were estimated by energy dispersive spectroscopy (EDS). The average compositions do not vary from grain to grain in the $Zr_{0.8}Nd_{0.2}O_{1.9}$ sample, indicating a single-phase microstructure. Further, the overall composition (Zr: Nd = 0.78: 0.22, determined over an area of 2 mm × 2 mm) is in excellent agreement with the nominal compositions taken for combustion synthesis of $Zr_{0.8}Nd_{0.2}O_{1.9}$. To determine the solubility of Mg^{2+} in the $Zr_{0.8}Nd_{0.2}O_{1.9}$ phase in $Zr_{0.8}Nd_{0.2}O_{1.9}$–MgO composite sample, EDS was carried out in point acquisition mode. A representative BSE micrograph of the composite sample of higher magnification is shown in Fig. 3(d) for better clarity. The bright (spot-1) and dark (spot-2) phases in the micrograph correspond to $Zr_{0.8}Nd_{0.2}O_{1.9}$ (Mg-doped) and pure MgO phase, respectively, as confirmed with EDS results. Elemental analysis on the bright phase indicated ~6 atom% Mg^{2+} incorporation in F-type $Zr_{0.8}Nd_{0.2}O_{1.9}$ phase. Based on EDS analysis, the composition of the F-type phase was calculated as $Zr_{0.75}Nd_{0.19}Mg_{0.06}O_{1.845}$, where oxygen content was arrived at considering the charge balance requirement. On the other hand, the MgO phase was found to exist as a pure phase. EDS

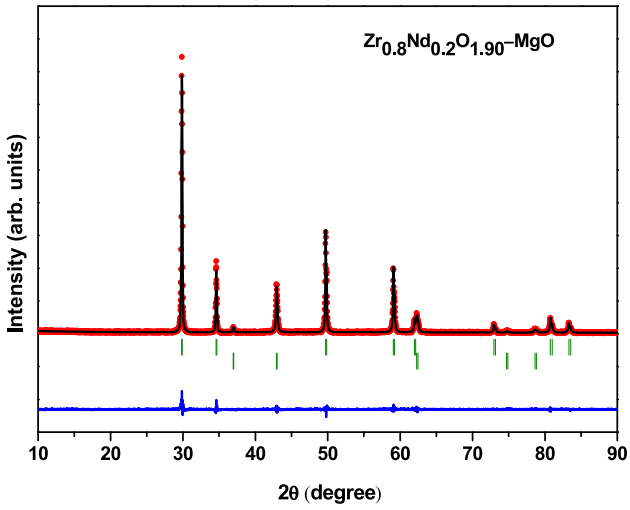

Fig. 2. Observed (red data points) and calculated (black fit curve) powder XRD patterns of $Zr_{0.8}Nd_{0.2}O_{1.9}$–MgO composite. Vertical lines indicate Bragg positions for fluorite type phase of $Zr_{0.8}Nd_{0.2}O_{1.9}$ and rock salt phase of MgO (top to bottom). The difference plot between observed and calculated pattern is also shown at the bottom (blue curve). (For interpretation of the references to colour in this figure legend, the reader is referred to the Web version of this article.)

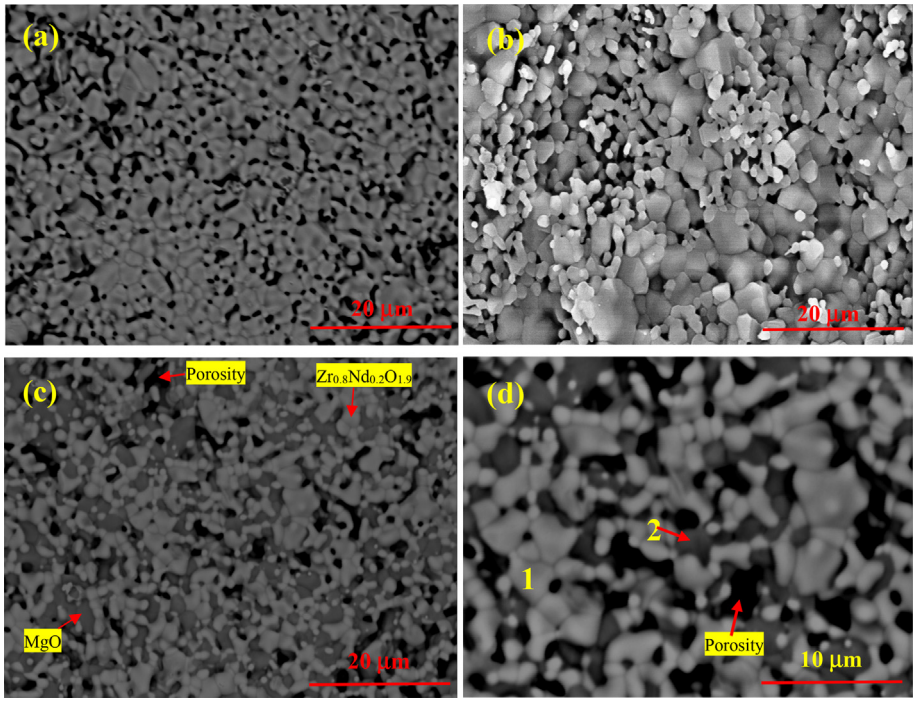

Fig. 3. BSE images of (a) $Zr_{0.8}Nd_{0.2}O_{1.9}$, (b) MgO, (c) $Zr_{0.8}Nd_{0.2}O_{1.9}$–MgO (50 wt %) composite and (d) magnified view of Fig. 3(c).

analysis, therefore, corroborated the findings of XRD results. At this point, it may be noted that we did observe slight solubility (2–3 atom%) of Zr^{4+} in MgO in our earlier paper [11] using EDS analysis. Serena et al. [31] also reported feeble solubility of ZrO_2 in MgO based on results obtained using electron probe micro-analysis coupled with X-ray spectrometry (EPMA-WDS). The very low solubility of ZrO_2 in MgO has been reported by a few other groups as well [32,33]. However, the EDS analysis of the present samples did not indicate the presence of Zr/Nd in the MgO phase. The discrepancy in results may be due to the gold coating of samples, which has overlapping peaks with Zr, particularly when the concentration of Zr is low.

3.2. Thermophysical property measurements

Understanding of thermophysical behaviour is an essential requirement to qualify a material envisaged for nuclear reactor applications. With this objective, high temperature linear thermal expansion, specific heat capacity and thermal conductivity of $Zr_{0.8}Nd_{0.2}O_{1.9}$, MgO and their composite (50 wt%) were evaluated. All measurements were carried out on sintered samples having a geometrical density of more than 80% of theoretical density (TD) (Table 2). These results are presented in the following section:

3.2.1. Thermal expansion studies

Accurate measurement of thermal expansivitiy of nuclear fuel materials is required to estimate the extent of swelling under thermal stress in order to optimize the fuel-clad gap and avoid fuel clad mechanical interactions (FCMI). Percentage linear thermal expansion ($100 \times \frac{\Delta L}{L}$) of $Zr_{0.8}Nd_{0.2}O_{1.9}$, $Zr_{0.8}Nd_{0.2}O_{1.9}$–MgO composite and MgO over 423 K–1573 K is plotted in Fig. 4. Experimentally determined results were fitted into second order polynomial functions and the following equations were obtained:

$Zr_{0.8}Nd_{0.2}O_{1.9}$

$$100\,x\,\frac{\Delta L}{L} = -0.30563 + 9.09239 \times 10^{-4}\,T + 1.37085 \times 10^{-7}\,T^2\,(423\,K - 1573\,K) \quad (1)$$

$Zr_{0.8}Nd_{0.2}O_{1.9}$–MgO

$$100\,x\,\frac{\Delta L}{L} = -0.37082 + 0.00104 \times T + 1.77953 \times 10^{-7}\,T^2\,(423\,K - 1573\,K) \quad (2)$$

MgO

$$100\,x\,\frac{\Delta L}{L} = -0.45299 + 0.00127 \times T + 1.56026 \times 10^{-7}\,T^2\,(423\,K - 1573\,K) \quad (3)$$

The average linear thermal expansion coefficient (α_L) is defined as

$$\alpha_L = \left(\frac{1}{L_o}\right)\frac{\Delta L}{\Delta T} \quad (4)$$

Where L_o is the length of the specimen at T_o, ΔL is the change in length and ΔT is the change in temperature. Values of 'α_L' for $Zr_{0.8}Nd_{0.2}O_{1.9}$, $Zr_{0.8}Nd_{0.2}O_{1.9}$–MgO composite and MgO (as evaluated from equation-4) are 11.5×10^{-6}/K, 13.4×10^{-6}/K and 15.1×10^{-6}/K, respectively, over the temperature range from RT to 1573 K. Thermal expansion of MgO has been investigated independently by many researchers by employing dilatometry [34,35], high-temperature X-ray diffraction [36,37] as well as theoretical studies [38]. Nielsen et al. [34] reported $\alpha_L = 15.2 \times 10^{-6}$/K to 15.4×10^{-6}/K for MgO over the temperature range from 298 K to 1473 K. Suzuki et al. [35] observed a higher expansion coefficient of 16.8×10^{-6}/K at 1573 K for highly pure MgO single crystal (>99.9% TD) and 15.9×10^{-6}/K at the same temperature for a low-density

Table 2
Dimensions, density and fractional porosity of sintered pellets employed for different studies. The standard deviation has been given in parenthesis.

Sample	Experiment	Dimensions of specimen (mm)		Measured density (g/cc)	Theore-tical density (g/cc)	% TD	Fractional porosity according to Eq. 7
		Height	Diameter				
$Zr_{0.8}Nd_{0.2}O_{1.90}$	Dilatometry	6.55 (0.03)	7.03 (0.04)	5.53 (0.07)	6.25	88	0.12
	Thermal diffusivity	1.51 (0.04)	10.05 (0.06)	5.35 (0.15)		86	0.14
MgO	Dilatometry	7.19 (0.02)	6.91 (0.07)	2.97 (0.04)	3.58	83	0.17
	Thermal diffusivity	1.42 (0.07)	10.74 (0.07)	2.83 (0.07)		79	0.21
$Zr_{0.8}Nd_{0.2}O_{1.90}$–MgO (50 wt %)	Dilatometry	5.11 (0.02)	6.99 (0.08)	4.15 (0.07)	4.55	91	0.09
	Thermal diffusivity	1.33 (0.03)	10.61 (0.05)	4.13 (0.09)		91	0.09

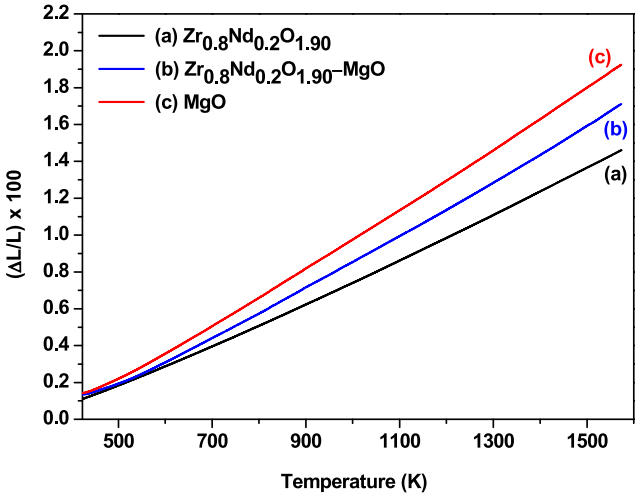

Fig. 4. Temperature-dependent fractional linear thermal expansion behaviour of (a) $Zr_{0.8}Nd_{0.2}O_{1.9}$, (b) $Zr_{0.8}Nd_{0.2}O_{1.9}$–MgO composite and (c) MgO.

synthetic sample (>92.4% TD) and highlighted the dependence of bulk thermal expansion coefficient on sample density. It may be noted here that the density of MgO sample used in the present study is further lower (~2.97 g/cc; > 82.9% TD), and therefore, the observed average thermal expansion coefficient (15.1×10^{-6}/K) is in line with the density dependence trend of the same. Dubrovinsky et al. [36] reported molar volume of MgO as 11.2434 cm^3 and 11.9081 cm^3 at 298 K and 1598 K, respectively, using *in situ* HT-XRD studies. Using these data, the lattice thermal expansion coefficient of MgO over the temperature range from 298 K to 1598 K was evaluated to be 14.9×10^{-6}/K. Fiquet et al. [37] also reported an expansion coefficient for MgO (15.6×10^{-6}/K) based on the measured molar volume of 11.227 cm^3 and 11.903 cm^3 at 298 K and 1557 K, respectively. A similar value of thermal expansion coefficient (15.6×10^{-6}/K) for MgO has been reported by Rao et al. [39] over 300 K–1250 K. On the other hand, using computational tools, Reeber et al. [38] calculated a higher expansion coefficient (16.8×10^{-6}/K) over the temperature range from 300 K to 1500 K. Results obtained on MgO in the present investigation are well compared to above-cited literature information and therefore validates the acceptability of our results on pure MgO. Similar to MgO, literature information is available for the thermal expansion behavior of $Zr_{0.8}Nd_{0.2}O_{1.9}$. Liu et al. [15] have reported a linear bulk thermal expansion coefficient for $Zr_{0.8}Nd_{0.2}O_{1.9}$ (~11.5×10^{-6}/K) over the temperature range from 300 K to 1573 K, which matches well with present results. It can be seen that the addition of 50 wt% MgO to $Zr_{0.8}Nd_{0.2}O_{1.9}$ to form $Zr_{0.8}Nd_{0.2}O_{1.9}$–MgO composite leads to an increase in average linear thermal expansion coefficient from 11.5×10^{-6}/K (for $Zr_{0.8}Nd_{0.2}O_{1.9}$) to 13.4×10^{-6}/K (for $Zr_{0.8}Nd_{0.2}O_{1.9}$–MgO composite). This increase is attributed to higher thermal expansivity of MgO as compared to that of $Zr_{0.8}Nd_{0.2}O_{1.9}$. The thermal expansion coefficient for $Zr_{0.8}Nd_{0.2}O_{1.9}$–MgO (50 wt% or 63.58 vol% MgO) composite was estimated to be 13.8×10^{-6}/K employing the rule of mixture using the following equation [40]:

$$\alpha_{Composite} = \alpha_{MgO} \times V_{MgO} + \alpha_{ZrNdO} \times V_{ZrNdO}$$

where $\alpha_{Composite}$, α_{MgO} and α_{ZrNdO} are the thermal expansion coefficients of composite, pure MgO and $Zr_{0.8}Nd_{0.2}O_{1.9}$, respectively; and V_{MgO} and V_{ZrNdO} are the volume fractions of pure MgO and $Zr_{0.8}Nd_{0.2}O_{1.9}$, respectively. It was found that the experimentally determined thermal expansion coefficient is approximately 3% lower as compared to that determined by the rule of mixture, which does not consider any interaction the constituent phases. The authors, therefore, speculate that the homogeneous distribution of $Zr_{0.8}Nd_{0.2}O_{1.9}$ grains restrain the expansion of MgO grains in composite to some extent. Literature also indicates an increase in the thermal expansion coefficient upon the addition of MgO to neodymium zirconates [22]. Linear thermal expansion data has also been used to evaluate the temperature-dependent density of samples, which is required for the calculation of thermal conductivity. This has been discussed later in this manuscript.

3.2.2. Specific heat capacity studies

The main objective of calorimetric studies was to measure the mean specific heat capacity of $Zr_{0.8}Nd_{0.2}O_{1.9}$, $Zr_{0.8}Nd_{0.2}O_{1.9}$–MgO composite (50 wt%) and pure MgO. Specific heat measurements were repeated three times and the mean value of measurements at each temperature was taken as the average specific heat. The standard deviation was found to be within ± 2%. Experimentally measured specific heat capacities of $Zr_{0.8}Nd_{0.2}O_{1.9}$, MgO and their composite (50 wt %) are shown in Fig. 5. Specific heat data for MgO taken from Barin et al. [41] is also included for comparison. These results show that the measured specific heat of MgO is in excellent agreement (within ± 1%) with the literature values over the temperature range from 400 K to 1073 K [41,42]. MgO has the highest specific heat while $Zr_{0.8}Nd_{0.2}O_{1.9}$ exhibits the lowest specific heat. $Zr_{0.8}Nd_{0.2}O_{1.9}$–MgO composite shows intermediate values between the two constituents. Specific heat for the composite sample has also been estimated based on the experimentally determined specific heat of $Zr_{0.8}Nd_{0.2}O_{1.9}$ and MgO employing Neumann-Kopp's rule (weighted fractional sum of specific heats of components). Results show a very good match (within ± 3%) between estimated and measured values for the composite sample. Therefore, in the absence of experimental heat capacity data of various

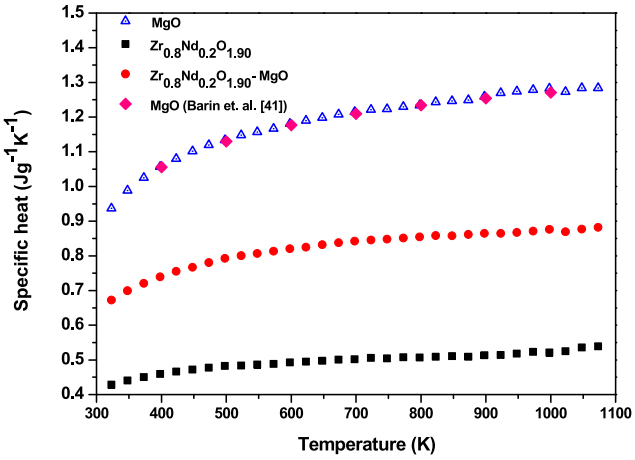

Fig. 5. Specific heat capacities of $Zr_{0.8}Nd_{0.2}O_{1.9}$, $Zr_{0.8}Nd_{0.2}O_{1.9}$–MgO composite and MgO as a function of temperature. Error bars are comparable to symbol size and hence not shown. Literature reported specific heat capacity of MgO [41] is also plotted along for comparison.

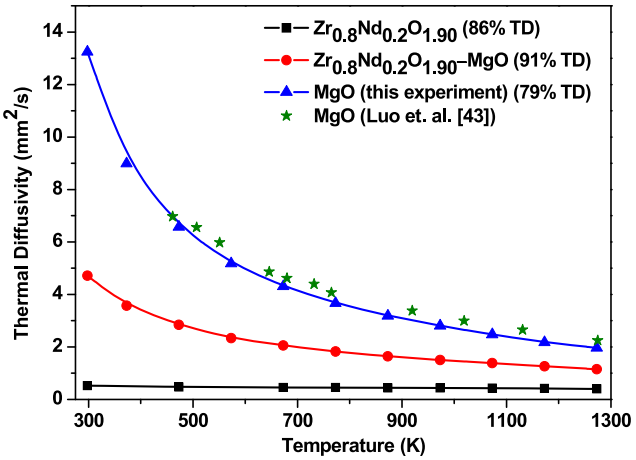

Fig. 6. As measured thermal diffusivity of $Zr_{0.8}Nd_{0.2}O_{1.9}$, $Zr_{0.8}Nd_{0.2}O_{1.9}$–MgO composite and MgO as a function of temperature. Error bars are comparable to symbol size and hence not shown. Literature reported thermal diffusivity of MgO [43] is plotted along for comparison.

compositions in the $Zr_{0.8}Nd_{0.2}O_{1.9}$–MgO system, estimated data using Neumann–Kopp rule may closely represent the true heat capacity of these composites. For all samples, specific heat increases with increasing temperature and does not exhibit any anomaly, thereby ruling out any phase transition over the investigated temperature range. Experimentally measured specific heat data was fit into $A + BT + CT^{-2}$ polynomial where A, B, and C are polynomial coefficients, and T is the absolute temperature. The values of these coefficients are given in Table 3. Specific heat capacity data has been used for the evaluation of thermal conductivity, which is discussed in the next section.

3.2.3. *Thermal diffusivity and conductivity studies*

Information on the thermal conductivity of materials envisaged to be used in nuclear reactors is of great importance. In the present investigation, thermal conductivities of $Zr_{0.8}Nd_{0.2}O_{1.9}$, its composite with 50 wt% MgO and pure MgO have been reported over the temperature range from RT to 1273 K. Thermal conductivity ($\lambda(T)$) was calculated from thermal diffusivity (D(T)), specific heat capacity ($C_P(T)$) and temperature-dependent density ($\rho(T)$) data using equation (5).

$$\lambda(T) = D(T) \times C_p(T) \times \rho(T) \quad (5)$$

Variation in the as-measured thermal diffusivity of all three samples as a function of temperature is shown in Fig. 6. Thermal diffusivity value at each temperature has been obtained by taking the arithmetic mean of three different measurements. The relative standard deviation was found to be $< \pm$ 3% based on these measurements. It was observed that the addition of MgO to $Zr_{0.8}Nd_{0.2}O_{1.9}$ leads to an increase in thermal diffusivity, as shown by diffusivity results of $Zr_{0.8}Nd_{0.2}O_{1.9}$–MgO composite. MgO shows the highest thermal diffusivity among all the three studied samples. Thermal diffusivity of MgO measured by Luo et al. [43] using the laser flash technique has also been incorporated in Fig. 6 for comparison. While the trend in diffusivity variation with temperature is similar in both cases, values reported by Luo et al. [43] are slightly higher than our results, which can be attributed to a higher density of MgO sample used by them (~93% TD) as compared to our sample (~79% TD). It was observed that thermal diffusivity data follow the inverse temperature dependence behaviour for all three samples, which indicates dominant phonon conduction behaviour; most common for insulating ceramics in the studied temperature range. It may be noted that the temperature dependence of diffusivity is less pronounced in the case of $Zr_{0.8}Nd_{0.2}O_{1.9}$. Temperature-dependent density '$\rho(T)$' was calculated from room temperature density and linear thermal expansion data. Here it must be mentioned that the uncertainty in the geometrical density of samples is approximately 3%. Further, an uncertainty of 2% in the thermal expansion data does not significantly influence the uncertainty in temperature-dependent volume and hence temperature-dependent density. Therefore, the uncertainty in temperature-dependent density is approximately 3%. The specific heat data required for the evaluation of thermal conductivity was calculated using specific heat equations given in Table 3. Estimated thermal conductivity decreased with increasing temperature except for $Zr_{0.8}Nd_{0.2}O_{1.9}$, where it showed nearly temperature-independent behaviour. The uncertainty in thermal diffusivity and specific heat values are 3% and 2%, respectively, as stated earlier. Therefore, the uncertainty of thermal conductivity values was estimated to be approximately 5% following the rule of propagation of uncertainties. Since the samples used for measurements were not fully dense, porosity correction was applied to the evaluated thermal conductivity data (λ_m) to arrive at the conductivity values of fully dense (100% TD) compositions (λ_{100}). Porosity correction was carried out using the following relation, which has widely been used for similar ceramics [15,44]:

Table 3
The coefficients of the specific heat equation for $Zr_{0.8}Nd_{0.2}O_{1.9}$, MgO and $Zr_{0.8}Nd_{0.2}O_{1.9}$–MgO composite.

Composition	(323–1073 K)		
	A	B	C
$Zr_{0.8}Nd_{0.2}O_{1.9}$	0.48143	0.00005	- 6807.19876
MgO	1.20909	0.00010	−31011.05917
$Zr_{0.8}Nd_{0.2}O_{1.9}$–MgO	0.85442	0.00004	- 20548.95794

$$\frac{\lambda_m}{\lambda_{100}} = 1 - \frac{4}{3}P \quad (6)$$

Here, 'P' is fractional porosity, which was calculated from theoretical density (ρ_t) and measured density (ρ_m) using equation (7).

$$P = \frac{\rho_t - \rho_m}{\rho_t} \quad (7)$$

Porosity corrected thermal conductivities of all studied samples as functions of temperature are shown in Fig. 7. Similar to thermal diffusivity, thermal conductivity also decreases with increasing temperature. These results also show that $Zr_{0.8}Nd_{0.2}O_{1.9}$ has very low thermal conductivity (~1.5 $Wm^{-1}K^{-1}$ (RT–1473 K)) and is weakly dependent on temperature [9,15]. Low thermal conductivity of Nd-substituted zirconia reported by many researchers [9,14,15,44], has been attributed to (i) large differences in mass and size between Zr^{4+} and Nd^{3+} ions, (ii) presence of oxygen ion vacancies and (iii) extensive structural disorder. On the contrary, MgO exhibits the highest thermal conductivity among all three samples studied here. For comparison, literature reported thermal conductivity values of MgO [43,45,46] are plotted along with results obtained in the present investigation. Slifka et al. [45] and Luo et al. [43] have reported thermal conductivity of the MgO sample having 93% and 98% theoretical density (TD), respectively, over the temperature range from 400 K to 1300 K. These values were normalized for fully dense specimens (100% TD; equation (6)) before plotting in Fig. 7. Results obtained on MgO in the present investigation were also compared with recommended conductivity values [46]. From Fig. 7, it is clear that the results obtained in this study are in good agreement with both literature reports as well as recommended values for MgO. It was also observed that the thermal conductivity of $Zr_{0.8}Nd_{0.2}O_{1.9}$ increases upon MgO addition. To be more precise, the thermal conductivity of the $Zr_{0.8}Nd_{0.2}O_{1.9}$ sample at room temperature increases from ~1.5 $Wm^{-1}K^{-1}$ to ~14 $Wm^{-1}K^{-1}$ upon 50 wt% addition of a highly thermally conductive MgO (46 $Wm^{-1}K^{-1}$ at RT) phase. The increase in thermal conductivity by approximately nine times (× 9) in $Zr_{0.8}Nd_{0.2}O_{1.9}$–MgO (50 wt%) composite as compared to phase pure $Zr_{0.8}Nd_{0.2}O_{1.9}$ may be ascribed to percolation theory [47]. According to this theory, a composite system composed of randomly mixed thermally more conductive and insulator phases exhibits a significant increase in thermal conductivity when the volume fraction of the highly conductive component is higher than a critical concentration, which is known as percolation threshold [48,49]. The higher is the thermal conductivity of the conductive component, higher will be the effective conductivity of the composite. In the present scenario, MgO (conductive component) exists as an almost pure phase and is advantageous for their applications in inert matrix fuel. To elaborate, if there is a considerable solubility of Zr^{4+} or Nd^{3+} in MgO, lots of lattice defects will be generated. These defects will act as phonon scattering centers. This would lead to decrease in thermal conductivity of MgO and consequently the composite. The decrease in thermal conductivity in substituted MgO has been confirmed by Kim et al. [50], who have reported thermal conductivity of 10 and 30 mol% Zn doped MgO, which is just 8.14 $Wm^{-1}K^{-1}$ and 4.79 $Wm^{-1}K^{-1}$, respectively, at room temperature. An increase in thermal conductivity has been reported in ZrO_2–MgO and Er-substituted ZrO_2–MgO system upon successive MgO addition [17]. More importantly, the thermal conductivity of $Zr_{0.8}Nd_{0.2}O_{1.9}$–MgO composite is sufficiently higher (~14 $Wm^{-1}K^{-1}$ at RT, ~10.4 $Wm^{-1}K^{-1}$ at 473 K and ~4.6 $Wm^{-1}K^{-1}$ at 1273 K) than that of a highly dense UO_2 (~8.7 $Wm^{-1}K^{-1}$ at RT, ~6.8 $Wm^{-1}K^{-1}$ at 473 K and ~3.1 $Wm^{-1}K^{-1}$ at 1273 K) sample [51], which is industrially used conventional ceramic oxide nuclear fuel worldwide.

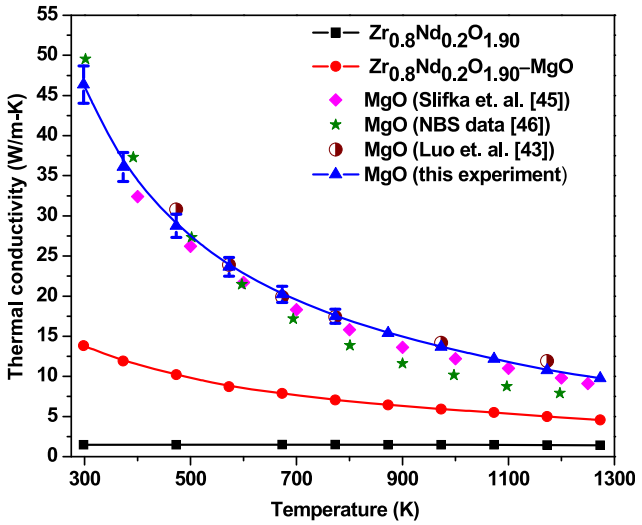

Fig. 7. Porosity corrected thermal conductivity of $Zr_{0.8}Nd_{0.2}O_{1.9}$, $Zr_{0.8}Nd_{0.2}O_{1.9}$–MgO composite and MgO samples as a function of temperature. Error bars represent one standard deviation (1σ) and are omitted where comparable or smaller to symbol size. Literature reported thermal conductivities of MgO [43,45,46] are also plotted along for comparison.

Present results of thermophysical properties clearly demonstrate high thermal conductivity of $Zr_{0.8}Nd_{0.2}O_{1.9}$–MgO composite (50 wt%) as compared to zirconia-based materials and make it a potential inert matrix fuel candidate for future reactor systems; particularly envisaged for minor actinide transmutation purpose.

4. Conclusion

$Zr_{0.8}Nd_{0.2}O_{1.9}$ was synthesized via the gel combustion route and $Zr_{0.8}Nd_{0.2}O_{1.9}$–MgO composite was prepared by a solid-state reaction of $Zr_{0.8}Nd_{0.2}O_{1.9}$ and commercially available MgO powders. $Zr_{0.8}Nd_{0.2}O_{1.9}$, MgO and their composite (50 wt%) were thoroughly phase characterized by XRD. The marginal solubility of Mg^{2+} in the $Zr_{0.8}Nd_{0.2}O_{1.9}$ phase and existence of a pure MgO in the composite was confirmed by XRD in conjunction with EDS analysis. Reasonable open porosity was observed in the microstructure, which indicates the samples were not highly dense. The thermophysical properties of composite as well as the end members were investigated. The thermal expansion coefficient of the composite (13.4 × 10^{-6}/K) was observed to be intermediate between that of $Zr_{0.8}Nd_{0.2}O_{1.9}$ (11.5 × 10^{-6}/K) and MgO (15.1 × 10^{-6}/K). Specific heat capacity as a function of temperature has been evaluated for all three samples, which indicated an increase in specific heat with the addition of MgO to $Zr_{0.8}Nd_{0.2}O_{1.9}$. The highlight of the study is the significant enhancement of the thermal conductivity of $Zr_{0.8}Nd_{0.2}O_{1.9}$ by the addition of MgO as a secondary phase. Measured thermal conductivity of $Zr_{0.8}Nd_{0.2}O_{1.9}$–MgO (50 wt%) composite is more than that of conventional high density typical UO_2 fuel, thus justifying the potential of $Zr_{0.8}Nd_{0.2}O_{1.9}$–MgO composites as inert matrix fuel for minor actinides transmutation.

Declaration of competing interest

The authors declare that they have no known competing financial interests or personal relationships that could have appeared to influence the work reported in this paper.

Acknowledgment

The authors would like to thank Mr. Vivek Bhasin, Director, Nuclear fuels Group, Bhabha Atomic Research Centre, for his valuable suggestions and useful discussion regarding this work.

Appendix A. Supplementary data

Supplementary data to this article can be found online at https://doi.org/10.1016/j.net.2020.07.022.

Data availability

The relevant data will be made available on request.

References

[1] H. Shahbunder, A.A. Al Qaaod, E.A. Amin, S. El-Kameesy, Effects of Pu and MA uniform and nonuniform distributions on subcritical multiplication of TRIGA Mark II ADS reactor, Ann. Nucl. Energy 94 (2016) 332–337.

[2] G. Alonso, E. Martinez, J.R. Ramírez, H. Hernandez, Radiotoxicity implications and reduction strategies of minor actinide in a boiling water reactor, Ann. Nucl. Energy 99 (2017) 410–420.

[3] C. Degueldre, J. Paratte, Concepts for an inert matrix fuel, an overview, J. Nucl. Mater. 274 (1999) 1–6.

[4] H. Kleykamp, Selection of materials as diluents for burning of plutonium fuels in nuclear reactors, J. Nucl. Mater. 275 (1999) 1–11.

[5] V. Anastasov, M. Betti, F. Boisson, F. Depisch, F. Houlbreque, R. Jeffree, I. Khamis, S. Lattemann, J. Miquel, S. Nisan, Status of Minor Actinide Fuel Development, IAEA Nuclear energy series No, 2009. NF-T-4.6.

[6] F. Sokolov, H. Nawada, Viability of Inert Matrix Fuel in Reducing Plutonium Amounts in Reactors, International Atomic Energy Agency, 2006, p. 1.

[7] P. Raison, R. Haire, Structural investigation of the pseudo-ternary system AmO_2–Cm_2O_3–ZrO_2 as potential materials for transmutation, J. Nucl. Mater. 320 (2003) 31–35.

[8] C. Degueldre, Zirconia inert matrix for plutonium utilisation and minor actinides disposition in reactors, J. Alloys Compd. 444 (2007) 36–41.

[9] C. Nandi, D. Jain, V. Grover, K. Krishnan, J. Banerjee, A. Prakash, K. Khan, A. Tyagi, ZrO_2-$NdO_{1.5}$ system: investigations of phase relation and thermophysical properties, Mater. Des. 121 (2017) 101–108.

[10] C. Nandi, D. Jain, V. Grover, R. Dawar, S. Kaity, A. Prakash, A. Tyagi, $Zr_{0.70}[Y_{1-x}Nd_x]_{0.30}O_{1.85}$ as a potential candidate for inert matrix fuel: structural and thermophysical property investigations, J. Nucl. Mater. 510 (2018) 178–186.

[11] C. Nandi, V. Grover, P. Kulriya, A. Poswal, A. Prakash, K. Khan, D. Avasthi, A. Tyagi, Structural response of Nd-stabilized zirconia and its composite under extreme conditions of swift heavy ion irradiation, J. Nucl. Mater. 499 (2018) 216–224.

[12] M. Patel, V. Vijayakumar, S. Kailas, D. Avasthi, J. Pivin, A. Tyagi, Structural modifications in pyrochlores caused by ions in the electronic stopping regime, J. Nucl. Mater. 380 (2008) 93–98.

[13] G.R. Lumpkin, M. Pruneda, S. Rios, K.L. Smith, K. Trachenko, K.R. Whittle, N.J. Zaluzec, Nature of the chemical bond and prediction of radiation tolerance in pyrochlore and defect fluorite compounds, J. Solid State Chem. 180 (2007) 1512–1518.

[14] C. Nandi, D. Jain, V. Grover, R. Dawar, S. Kaity, A. Prakash, A. Tyagi, $Zr_{0.70}[Y_{1-x}Nd_x]_{0.30}O_{1.85}$ as a potential candidate for inert matrix fuel: structural and thermophysical property investigations, J. Nucl. Mater. 510 (2018) 178–186.

[15] Z.-G. Liu, J.-H. Ouyang, B.-H. Wang, Y. Zhou, J. Li, Preparation and thermophysical properties of $Nd_xZr_{1-x}O_{2-x/2}$ (x= 0.1, 0.2, 0.3, 0.4, 0.5) ceramics, J. Alloys Compd. 466 (2008) 39–44.

[16] S. Lutique, R. Konings, V. Rondinella, J. Somers, T. Wiss, The thermal conductivity of $Nd_2Zr_2O_7$ pyrochlore and the thermal behaviour of pyrochlore-based inert matrix fuel, J. Alloys Compd. 352 (2003) 1–5.

[17] P. Medvedev, M. Lambregts, M. Meyer, Thermal conductivity and acid dissolution behavior of MgO–ZrO_2 ceramics for use in LWR inert matrix fuel, J. Nucl. Mater. 349 (2006) 167–177.

[18] S. Miwa, M. Osaka, Oxidation and reduction behaviors of a prototypic MgO-PuO_{2-x} inert matrix fuel, J. Nucl. Mater. 487 (2017) 1–4.

[19] S. Yates, K. McClellan, J. Nino, The effect of processing on the thermal diffusivity of MgO–$Nd_2Zr_2O_7$ composites for inert matrix materials, J. Nucl. Mater. 393 (2009) 203–211.

[20] P. Medvedev, S. Frank, T. O'Holleran, M. Meyer, Dual phase MgO–ZrO_2 ceramics for use in LWR inert matrix fuel, J. Nucl. Mater. 342 (1–3) (2005) 48–62.

[21] J. Jung, H. Runge, The compatibility of basalt and MgO with liquid sodium, Liquid metal engineering and technology. 3 v, in: Proceedings of the 3. International Conference Held in Oxford on 9-13 April, 1984.

[22] A. Nelson, M. Giachino, J. Nino, K. McClellan, Effect of composition on thermal conductivity of MgO–$Nd_2Zr_2O_7$ composites for inert matrix materials, J. Nucl. Mater. 444 (2014) 385–392.

[23] E. Neeft, K. Bakker, R. Schram, R. Conrad, R. Konings, The EFTTRA-T3 irradiation experiment on inert matrix fuels, J. Nucl. Mater. 320 (2003) 106–116.

[24] N. Chauvin, T. Albiol, R. Mazoyer, J. Noirot, D. Lespiaux, J. Dumas, C. Weinberg, J. Menard, J. Ottaviani, In-pile studies of inert matrices with emphasis on magnesia and magnesium aluminate spinel, J. Nucl. Mater. 274 (1999) 91–97.

[25] G. Prasad, V. Sinha, P. Hegde, Development and fabrication of LEU plate fuel for modified core of APSARA reactor, BARC Newsletter 21 (2012).

[26] P. Dehaudt, A. Mocellin, G. Eminet, L. Caillot, G. Delette, M. Bauer, I. Viallard, Composite Fuel Behaviour under and after Irradiation, 1997. IAEA-TECDOC-970.

[27] N. Chauvin, T. Albiol, R. Mazoyer, J. Noirot, D. Lespiaux, J. Dumas, C. Weinberg, J. Menard, J. Ottaviani, In-pile studies of inert matrices with emphasis on magnesia and magnesium aluminate spinel, J. Nucl. Mater. 274 (1999) 91–97.

[28] J. RodriguezeCarvajal, Program FullProf. 2k (Version 5.00), Laboratoire Léon Brillouin, France, 2011.

[29] R.D. Shannon, Revised effective ionic radii and systematic studies of interatomic distances in halides and chalcogenides, Acta Crystallogr. A 32 (1976) 751–767.

[30] T. Noguchi, M. Mizuno, Liquidus curve measurements in the ZrO_2-MgO system with the solar furnace, B. Chem. Soc. Jap. 41 (1968) 1583–1587.

[31] S. Serena, M.A. Sáinz, Á. Caballero, Experimental determination and thermodynamic calculation of the zirconia–calcia–magnesia system at 1600, 1700, and 1750°C, J. Am. Ceram. Soc. 87 (2004) 2268–2274.

[32] D. Yong, J. Zhanpeng, Optimization and calculation of the ZrO_2-MgO system, Calphad 15 (1991) 59–68.

[33] H. Scott, Phase relations in the magnesia-yttria-zirconia system, J. Australas. Ceram. Soc. 17 (1981) 16–20.

[34] T. Nielsen, M. Leipold, Thermal expansion in air of ceramic oxides to 2200° C, J. Am. Ceram. Soc. 46 (1963) 381–387.

[35] I. Suzuki, Thermal expansion of periclase and olivine, and their anharmonic properties, J. Phys. Earth 23 (2) (1975) 145–159.

[36] L. Dubrovinsky, S. Saxena, Thermal expansion of periclase (MgO) and tungsten (W) to melting temperatures, Phys. Chem. Miner. 24 (8) (1997) 547–550.

[37] G. Fiquet, P. Richet, G. Montagnac, High-temperature thermal expansion of lime, periclase, corundum and spinel, Phys. Chem. Miner. 27 (1999) 103–111.

[38] R.R. Reeber, K. Goessel, K. Wang, Thermal expansion and molar volume of MgO, periclase, Eur. J. Mineral 7 (1995) 1039–1047.

[39] A. Rao, K. Narender, Studies on thermophysical properties of CaO and MgO by γ-ray attenuation, J. Thermodyn. 2014 (2014) 123478.

[40] L. Cheng, B. Yan, R. Gao, X. Liu, Z. Yang, B. Li, Y. Zhong, P. Liu, Y. Wang, M. Chu, Densification behaviour of UO_2/Mo core-shell composite pellets with a reduced coefficient of thermal expansion, Ceram. Int. 46 (2020) 4730–4736.

[41] I. Barin, G. Platzki, Thermochemical Data of Pure Substances, Wiley Online Library, 1989.

[42] D.R. Stull, H. Prophet, JANAF Thermochemical Tables, National Standard Reference Data System, 1971.

[43] J. Luo, R. Stevens, R. Taylor, Thermal diffusivity/conductivity of magnesium oxide/silicon carbide composites, J. Am. Ceram. Soc. 80 (1997) 699–704.

[44] L. Guo, Y. Zhang, F. Ye, Phase structure evolution and thermophysical properties of nonstoichiometry $Nd_{2-x}Zr_{2+x}O_{7+x/2}$ pyrochlore ceramics, J. Am. Ceram. Soc. 98 (2015) 1013–1018.

[45] A.J. Slifka, B.J. Filla, J. Phelps, Thermal conductivity of magnesium oxide from absolute, steady-state measurements, J. Res. Natl. Inst. Stand. Technol. 103 (1998) 357.

[46] R. Powell, C.Y. Ho, P.E. Liley, Thermal Conductivity of Selected Materials, US Department of Commerce, National Bureau of Standards Washington, DC, 1966.

[47] D. Stauffer, A. Aharony, Introduction to Percolation Theory, CRC press, 2018.

[48] G. Zhang, Y. Xia, H. Wang, Y. Tao, G. Tao, S. Tu, H. Wu, A percolation model of thermal conductivity for filled polymer composites, J. Compos. Mater. 44 (2010) 963–970.

[49] L. Kong, J. Zhang, Y. Maeda, M.G. Blackford, S. Li, G. Triani, D.J. Gregg, Novel synthesis and thermal property analysis of MgO–$Nd_2Zr_2O_7$ composite, Ceram. Int. 42 (2016) 16888–16896.

[50] Y. Kim, J. Lee, N. Kim, H.K. Yu, Thermal conductivity-controlled Zn-doped MgO/$Mg(OH)_2$ micro-structures for high-efficiency thermo-dynamic heat energy storage, J. Asian Ceram. Soc. 8 (2020) 50–56.

[51] P.L. Kirillov, Thermophysical Properties of Materials for Nuclear Engineering: Tutorial for Students of Specialty Nuclear Power Plants, OBNINSK INSTITUTE FOR ATOMIC POWER ENGINEERING, 2006.